Numerical Methods in Civil Engineering, 9-3 (2025) 63-74

Numerical Methods in Civil Engineering

Journal Homepage: https://nmce.kntu.ac.ir/

Finite Element Modeling of the Behavior of Hybrid-Fiber Reinforced Concrete under Tri-axial Compression

Ali Naserifar*

ARTICLE INFO

RESEARCH PAPER

Article history:
Received:
December 2023
Revised:
July 2024
Accepted:
March 2025

Keywords:
Fiber Reinforced;
Concrete, Constitutive;
Model, Tri-axial;
Behavior

Abstract:

Concrete is the most popular building material in the worldwide. However, its low tensile strength causes cracks to initiate in the low step of loading. Today, fibers of various types are used in concrete mixtures to improve the behavior of it. However, the behavior of fiber-reinforced concrete has been studied frequently but a numerical model that can predict the behavior of fiber-reinforced concrete well is under research. In this research, the integration algorithm of the structural equations and the implementation of the William-Warnke behavioral model for fiber-reinforced concrete are presented. The aforementioned behavioral model is coded and linked to ABQUS software as a subprogram and used in the analysis of boundary value problems. To carry out validation, several real triaxial tests have been simulated and compared with the results of real tests. The results show that the coded model simulates the laboratory behavior of fiber-reinforced concrete as well and can be used in modeling real projects.

1. Introduction

Concrete is widely used in construction and its global usage has been increasing. Traditional concrete often develops cracks due to its limited tensile strength and low shear strength, making it vulnerable to brittle failure under tension and shear if not reinforced. To prevent these failures, concrete needs adequate reinforcement, which is commonly achieved by using fibers. These fibers can be used as a substitute for or in conjunction with traditional steel reinforcement [1]. Extensive research studies have been carried out to address limitations and reduce dependency on steel reinforcing; however, the majority of innovations published so far are successful in using fiber-reinforced concrete (FRC) for effective reinforcement of concrete properties. [2, 3, 4, 5].

Nowadays, fiber concrete is commonly used in engineering structures such as high-rise buildings, bridges, dams, tunnels, and nuclear power plants. Steel, PP polypropylene, PE polyethylene, PVA Polyvinyl Alcohol, basalt fibers, carbon fiber, glass fiber, and aramid fiber are the most important fibers in use today [6]. Studies have demonstrated that incorporating fibers into concrete significantly enhances the flexibility of structural elements. Furthermore, it improves the environment for initiating cracks, toughness, maximum strength, resilience to impact and explosion, and shear resistance [1-6].

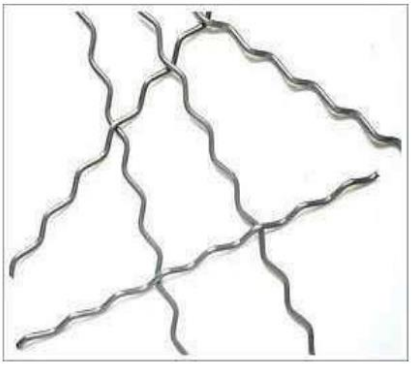

(a)

*Corresponding author: Assistant Professor, Faculty of Civil Engineering, Yadegare-e-Imam khomeini (RAH) Shahre Rey Branch, Islamic Azad University, Tehran, Iran.
Email: Ali.Naserifar@iau.ac.ir

https://doi.org/10.61186/NMCE.2312.1039

(b)

(c)

(d)

Fig. 1: Prospective features, (a) steel fiber, (b) PVA, (c) glass fiber, (d) polypropylene fibers [7].

Cucchiara, C. et al. in 2004 [8] investigated the effect of steel fibers on concrete shear strength. For this purpose, a four-point bending beam was tested, and depending on the amount of transverse rebar available, it was 0, 1, and 2%. Fibers were added to the mixture and the shear and bending failure mechanism was studied. The results showed that by using fibers the failure mechanism changes from shear to bending.

Dancygier, A. N. et al. [9] investigated the bending behavior of high-strength concrete that is reinforced with steel fibers and low rebar percentage. In their research, the specimens with 200*300*3900 mm were used for a four-point bending test and the volume of fiber was 0.75 percent. The results showed that by using steel fibers the failure mechanism changes from shear failure to bending one and the ductility of specimens has increased.

Holschemacher, K. et al. [10] investigated the effect of steel fibers on the mechanical behavior of high-strength concrete. The purpose of this study was the effect of the steel fibers on the bending and tension behavior of concrete. Three types of steel fibers including zigzag, smooth, and hook types were used in FRC.

Steel fibers can cause ductile behavior in high-strength concrete after cracking. In the concrete beams with smooth steel fibers, the fibers did not fail during the test but were pulled out from the concrete, while in the concrete that was reinforced with zigzag steel fibers, the fibers ruptured during the test without pulling out from the concrete. In the concrete beam samples that were reinforced with 0 and 20 kg/m^3, steel fiber shear failure occurred and for the samples with 40 kg/m^3 and without steel rebar the failure was compression type. For samples with longitudinal rebar and 60 kg/m^3 steel fibers, the failure was bending and compression type.

Olivito, R. S. [11] experimentally studied the uniaxial compression, tension, and bending strength of steel fiber reinforced by a four-point bending test. The steel fibers with 22, 30, and 40 mm lengths and 1 and 2 percent volume have been used in concrete mix and beam samples with 150x150x600 mm dimensions constructed for a four-point bending test. The results showed that because of an increase in the volume and length of the fiber, the ductility and energy absorption of the beam increased along with cracking. Beams with short steel fibers showed a softer behavior than beams with long fibers [11].

Ding, Y., and colleagues conducted a study in 2011 to explore how the combination of steel fibers and stirrups affects the shear behavior of fresh Self-Consolidating Concrete (SCC). Their findings suggest that increasing the fiber content notably enhances the shear strength. Moreover, adding steel fibers in appropriate proportions can shift the failure mode from a brittle shear collapse to a more flexible bending mechanism. This study also suggests that steel fibers can partially replace stirrups in this context [12].

Steel fibers increase the tensile strength of FRC and PP fibers prevent the explosive failure of FRC at high temperatures. Other fibers also affect the performance of FRC exposed to high temperatures. Considering that different fibers have different effects on the performance of concrete, it is better to use a combination of fibers today.

In Steel Fiber Reinforced Concrete (SFRC) beams lacking transverse reinforcement, four main mechanisms are responsible for resisting the total shear force. These include the compressed concrete in the compression zone, aggregate interlocking through the aggregate interface at the critical diagonal crack, dowel action by the longitudinal tension reinforcement, and steel fibers bridging the critical diagonal crack [13].

Due to relative progress in fiber-reinforced concrete manufacturing technology in recent decades, it has led to a

demand for sophisticated behavioral models that can accurately simulate and describe the performance of fiber-reinforced concrete under different load conditions. So far, considerable efforts have been dedicated to the development of behavioral models for both normal concrete and high-strength concrete [14, 15, 16, 17, 18, 19, 20, 21]. These researches include behavioral models that have been presented by using theories such as models based on the theory of plasticity, destruction models, micro-level models, and separate models. A variety of behavioral models have been extended to fiber-reinforced concrete with metal fibers by applying existing conventional models for conventional concrete [2, 22, 23, 24,]. The comparison between laboratory results and numerical simulations in complex problems shows that the use of estimated and calibrated behavioral models (behavioral models suitable for other materials that are calibrated from the stress paths for fiber concrete) leads to very imprecise results in expressing the behavior of fiber concrete [25, 26, 27, 28]. The study of previous research shows that a suitable behavioral model for fiber concrete should be affected by the physical and mechanical characteristics as well as the volume of the fibers used [29, 30, 31]. One of the effective behavioral models for predicting the behavior of normal concrete is the five-parameter William-Warnke behavioral model, which is included in commercial finite element software and used for modeling concrete structures. [32].

Yin Chi et al. [25] have presented a model that can be used for fiber concrete by using the effect of fiber characteristics on yield and hardening laws of the William-Warnke model. They showed that the behavior of fiber concrete compared to ordinary concrete shows certain complications such as strain softening/hardening, volume expansion, dependence on all-around pressure, etc., and is affected by the characteristics.

Slater, E. et al. [33] utilized a substantial database comprising 222 shear strength tests of steel fiber reinforced concrete beams (SFRC) without stirrups to formulate equations for forecasting the shear strength of concrete beams. Their research revealed that the linear regression equations derived from the SFRC database were successful in accurately forecasting shear strength when compared to previously proposed models.

Negi B. S. et al. [13] put forward a mechanics-based mathematical model that takes into account all shear-resisting mechanisms to predict the shear strength of steel fiber-reinforced concrete beams, along with recommending the contribution of each shear-resisting mechanism. On the other hand, Sabetifar et al. [34] introduced a semi-empirical model that utilizes the gene expression programming (GEP) technique to estimate the ultimate shear strength of steel fiber-reinforced concrete (SFRC) beams without shear reinforcement.

In this research, the implementation and structural integration algorithm of the behavioral model developed by William-Warnke for fiber concrete and have been introduced by Yin Chi et al. [45] investigated. Finally, the aforementioned behavioral model was coded as a UMAT subprogram and introduced to ABAQUS finite element software, verified by simulating real tri-axial tests and comparing them with experimental data, and used in problem analysis.

2. Constitutive behavior of FRC

For normal concrete, many constitutive models, by considering many theories such as the theory of plasticity, concrete damage plasticity model and micro-plane models have been introduced that can show the behavioral properties of concrete. The current equations of normal concrete can be considered as the basis of constitutive models for FRC. Some of these equations that have been introduced in the finite element software make it possible for researchers to use these models in the investigation of the mechanical behavior of concrete.

In recent decades, many studies have been done to investigate the behavior of FRC under multi-axial stresses and developing constitutive models [16,35]. Pantazopoulou, S. J. et al. investigated the triaxial behavior of FRC for the first time in 2001 and developed the constitutive properties of FRC following the fiber type, fiber percentage, load path, test condition, and sample size through experiments on 250 samples [36]. Farnam, Y. et al. in 2010 investigated the effect of lateral pressure increase on the ductility and plastic behavior of FRC [37]. Also, Fi Jiang et al. experimentally worked on FRC under a variety of uniform loading protocols with different confinement pressures and completed the stress path [38]. Complications of triaxial tests and dependence of test results on very parameters necessitate the use of constitutive equations for accurate modeling of the FRC behavior under multi-axial stresses [14, 24, 39, 40]. Another model that has been introduced for modeling concrete behavior is the five-parameter William-Warnke model, which is one of the most advanced and accurate models to simulate concrete behavior but has not been introduced in finite element software and is not usable [41]. In the study that Yin and Chia did on the behavior of triaxial behaviors of FRC at Nottingham University in 2012, they achieved a variety of equations for the FRC constitutive model. In this study, the steel fibers were used in combination with Polypropylene fibers to improve the

behavior of concrete, and the five-parameter William-Warnke model was used for modeling concrete [42].

Based on the results of the Barcelona test and considering concrete tension strength, Blanco, A. et al., proposed constitutive equations for concrete and compared the results of numerical modeling with the experimental ones and the euro code [43].

Mihai, I. C. et al. have presented the constitutive model of concrete based on the concrete damage plasticity method. This model was based on sub-models mechanical behavior to model crack direction, crack surface performance, and translating the crack by fibers through both sides of sub-crack. In their study, the developed constitutive models were based on the concrete strength after cracking of fiber-reinforced concrete in the bending test [44].

Chi, Y. et al. [42] developed a plasticity constitutive model for hybrid steel-polypropylene fiber reinforced concrete (HFRC) based on 75 true triaxial compression tests on cubic specimens to predict the strength and deformation of HFRC under various loading conditions. In their study, they modified a five-parameter Willam-Warnke failure surface to account for the presence of hybrid fibers. The loading surface's evolution is characterized by uncoupled hardening and softening regimes determined by the accumulated equivalent plastic strain and a Drucker-Prager non-associated plastic flow is employed to describe the plastic deformation [45].

A model by Liang, X. et al. was developed for the numerical investigation of FRC. In this model, the mechanical model of concrete and fibers is considered separately and the interaction between fibers and concrete is modeled by the fiber interaction surface [46].

According to the author's knowledge and research, there is not any predefined FRC behavior model in the popular finite element software such as ATENA, ANSYS, and ABAQUS, so yet. So, in this study, the FRC behavior model in the form of user subroutine code is introduced to ABAQUS finite element software.

2.1 Developed William -Warnke five parameters model for FRC

As said, in this study, the FRC behavior model in the form of user subroutine code is introduced to ABAQUS finite element software. The general algorithm of ABAQUS software using UMAT is shown in Figure 2.

2.2 The behavioral model of William-Warnke for fiber concrete

In formulating the rupture criterion for concrete under multi-axial stresses, it should be noted that the selected criterion is under the basic laws of thermodynamics, and also based on the laboratory results. It should be a correct estimate of rupture. Many rupture criteria have been proposed to check concrete under multi-axial stresses, but the developed five-parameter William-Warnke model for fiber concrete (HFRC-WW) is more realistic and has better compliance with laboratory results [25]. In this model, the effects of fiber addition are applied through the fiber index parameter (FRI), which can consider the effect of steel and polymer fibers. Also, the physical and geometric characteristics and the weight percentage of the fibers used in the behavioral model (HFRC-WW) are effective.

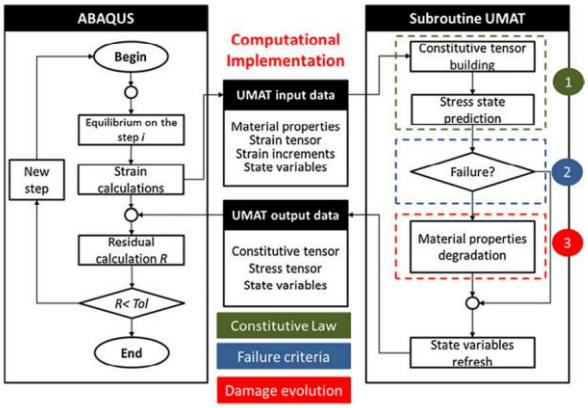

Fig. 2: The general algorithm of ABAQUS solver using UMAT [47]

2.3 Yield surface

The yield surface of the five-parameter William-Warnke generalized behavioral model for fiber concrete in Westergaard coordinates is as follows [25]:

$$f(\xi,\rho,\theta)=\sqrt{2J_2}-K(\bar{\varepsilon}_p)\rho^{hf}(\xi,\theta)=0 \tag{1}$$

Where $K(\bar{\varepsilon}_p)$ is the hardening/softening parameter that defines the increase of strength during hardening and the strength deterioration during softening. This is a function of

$$\rho^{hf}(\xi,\theta)=\frac{2\rho_c^{hf}(\rho_c^{hf^2}-\rho_t^{hf^2})\cos\theta}{4((\rho_c^{hf^2}-\rho_t^{hf^2})\cos^2\theta)+(\rho_c^{hf}-2\rho_t^{hf})^2}+\frac{\rho_c^{hf}(2\rho_t^{hf}-\rho_c^{hf})\sqrt{4((\rho_c^{hf^2}-\rho_t^{hf^2})\cos^2\theta)}}{4((\rho_c^{hf^2}-\rho_t^{hf^2})\cos^2\theta)+(\rho_c^{hf}-2\rho_t^{hf})^2}+\frac{5\rho_t^{hf^2}-4\rho_c^{hf}\rho_t^{hf}}{4((\rho_c^{hf^2}-\rho_t^{hf^2})\cos^2\theta)+(\rho_c^{hf}-2\rho_t^{hf})^2} \tag{2}$$

Which ρ_c^{hf} is a compressive meridian and is defined as follows:

$$\frac{\xi}{f_{cu}^{'}}=b_0+b_1\frac{\rho_c^{hf}}{f_{cu}^{'}}+b_2\left(\frac{\rho_c^{hf}}{f_{cu}^{'}}\right)^2 \tag{3}$$

Also ρ_t^{hf} , the tension meridian is defined as follows:

$$\frac{\xi}{f_{cu}^{'}} = a_0 + a_1 \frac{\rho_t^{hf}}{f_{cu}^{'}} + a_2 \left(\frac{\rho_t^{hf}}{f_{cu}^{'}} \right)^2 \quad (4)$$

In equation 1, $J_2 = \frac{1}{2} s_{ij} s_{ij}$ is the second invariant of the deviatoric stress tensor and $\xi = \frac{I_1}{\sqrt{3}}$, and $I_1 = \sigma_{11} + \sigma_{22} + \sigma_{33}$ is the first invariant of the stress tensor, also $\cos\theta = \frac{2\sigma_3 - \sigma_2 - \sigma_1}{2\sqrt{3}\sqrt{J_2}}$ is the Ladd angle in which $\sigma_3 \geq \sigma_2 \geq \sigma_1$.

In the above relations, a_0 b_1 ، b_0 ،a_2 ،a_1 ،and b_2 are the basic parameters of the five-parameter William-Warnke model. It should be noted that by applying the condition of the intersection of the compressive and tensile meridian at a point of the hydrostatic axis, the number of parameters is reduced to 5 [14]. In equation 2, ρ_c^{hf} and ρ_t^{hf} apply the effects of adding fibers in the shape of the yield surface and are defined by the following relations [47]:

$$\rho_t^{hf} = k_t \rho_t \quad (5)$$

Plastic strain and takes values between K_0 to 1. Before any plastic deformation occurs, the hardening parameter keeps a constant value of K, defining the initial yield surface that bounds the elastic region. In addition, the function $\rho(\xi, \theta)$ defines the parabolic shape of the meridian, which is interpolated between the compressive and tensile meridian by the Lode angle $\theta = 0$ and is calculated by the following relationship:

$$\rho_c^{hf} = k_c \rho_c \quad (6)$$

As shown in Figure 3, the yielding procedure of the developed HFRC-WW model is in the form of a convex cone in the main stress space and in the form of a rounded triangle in the deviatoric π-plane.

2.4 Plastic potential surface with non-associated flow rule

Determining the plastic strain tensor (the increment of plastic strain) plays a significant role in predicting material behavior because it is assumed that most plasticity parameters are a function of plastic strain. For concrete and other materials whose behavior depends on hydrostatic stress, generally, non-associated flow roles have been used [14]. At the WW-HFRC, the non-associated flow rule is used for fiber-reinforced concrete. The plastic potential function that is used in this model in the Westergaard coordinate for the plain concrete proposed on the base Grassl, P. et al. [20] model is as follows:

$$g = A\rho(\xi,\theta)^2 + B\rho(\xi,\theta) + \xi = 0 \quad (7)$$

The parameters of A and B in the plastic potential function, are calculated based on the value of axial strain at the maximum loading point of the axial pressure test and also plastic strain at the maximum stress of the triaxial pressure test [20].

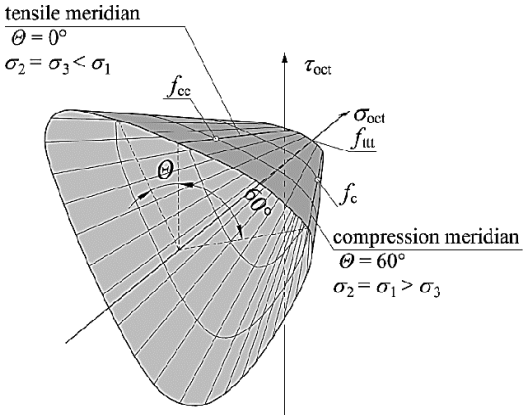

Fig. 3: The yield surface of the WWFRC constitutive model in the space of principal stresses.

2.5 Implementation of the behavioral model

The implementation of the behavioral model is done in the form of the UMAT subprogram, which is linked to the ABAQUS software. Integrating constitutive functions has been done using Euler's second-order explicit method, which is known as the substep method. In the substep method, using automatic division as an error control, the strain development is divided into some small steps and integrated from the constitutive equations, and the appropriate size of each step is determined through the modified Euler formula and compared with the defined error rate. In this study, for the integration of constitutive equations, the explicit step method based on the method proposed by Sloan et al. [48] was used. After integrating the constitutive equations and updating the stress position of the applied strain, finally, the elastoplastic tensor according to equation (8) is returned to the ABAQUS software, and the general equilibrium equation is solved in the form of nonlinear finite elements using the Newton-Raphson iteration method.

$$C_{ijkl}^{ep} = \left[C_{ijkl}^{e} - \frac{C_{ijmn}^{e} \frac{\partial G}{\partial \sigma_{mn}} \left(\frac{\partial F}{\partial \sigma_{pq}} \right)^T C_{pqkl}^{e}}{\left(\frac{\partial F}{\partial \sigma_{pq}} \right)^T C_{rstu}^{e} \frac{\partial G}{\partial \sigma_{tu}} - \frac{\partial F}{\partial K} \frac{\partial K}{\partial \varepsilon_{ij}^{p}} \frac{\partial G}{\partial \sigma_{ij}}} \right] \quad (8)$$

C^e is the elastic tensor of the material and is determined based on Hooke's rule, F is the yield function, G is the plastic potential function, and K is the hardening parameter.

2.6 Integration algorithm of HFRC-WW by sub-step method

The integration algorithm of the constitutive equations of the HFRC-WW behavior model for the increment of the applied strain $\Delta\varepsilon_{kl}^{tot}$ in the time step t is summarized below:

2.6.1 Prediction of the elastic strain

The entire increment of the applied strain is assumed to be elastic and its position on the yield surface is checked (FTOL is defined as user-oriented acceptable zero and a number between $10^{\wedge 6}$ and $10^{\wedge 12}$ is chosen).

$$\Delta\sigma^e = C^e \Delta\varepsilon^e \tag{9}$$

$$IF: F(\sigma_0 + \Delta\sigma^e, K_0) < FTOL \Rightarrow elastic\ step$$
$$\sigma_{new} = \sigma_0 + \Delta\sigma^e \tag{10}$$

2.6.2 Calculation of the location of the collision point of the elastic test stress with yield surface

If the applied strain increment caused plastic deformation, in other words, if $F(\sigma_0 + \Delta\sigma^e, K_0) > FTOL$, so the point of stress inclusion on the yield surface should be calculated. For this purpose, the below nonlinear equation is solved with iteration method and the value of scalar parameter α is calculated.

$$F(\sigma_0 + \alpha C^e \Delta\varepsilon, K_0) = F(\sigma_{intersection}, K_0) = 0 \tag{11}$$

In the above equation, if $\alpha = 0$, it means that $\Delta\varepsilon$ has led to a plastic deformation, and if $\alpha = 1$ it means that the deformation is completely elastic. For a transition from elastic to plastic state we have: $0<\alpha<1$ and the elastic part of the stress development is obtained from the relation $\alpha C^e \Delta\varepsilon$.

Equation 11 defines a nonlinear equation with the variable α that could be solved with different numerical methods such as the Secant method, Newton-Raphson method, etc. Newton-Raphson and Secant methods have a fast convergence rate but may cause divergence in some cases because they do not limit the solution to specific values of α. The Pegasus method presented by Dowell et al. is ideally suited for solving yield surface collision problems defined in equation (11) [49]. Since this method converges indefinitely, it does not need to use a derivative and converges in several finite steps.

2.7 Integration of constitutive equations and update of stress

For the increment of the applied strain $\Delta\varepsilon$, the structural equations that are integrated at each Gauss point of each element will be as follows:

STEP 1: Considering the initial quantity $T = 0$ and $\Delta T = 1$

STEP 2: Until T <1 repeat steps 3 to 10,

STEP 3: Calculate $\Delta\sigma_a$, $\Delta\sigma_b$, ΔK_a and ΔK_b based on this equation:

$$\Delta\lambda_a = \frac{\left(\frac{\partial F}{\partial \boldsymbol{\sigma}_0}\right)^T C^e \Delta\boldsymbol{\varepsilon}}{\left(\frac{\partial F}{\partial \boldsymbol{\sigma}_0}\right)^T C^e \frac{\partial G}{\partial \boldsymbol{\sigma}_0} - \sqrt{\frac{2}{3}} \frac{\partial F}{\partial K_0} H_p \left\| \frac{\partial G}{\partial \boldsymbol{\sigma}_0} \right\|} \tag{12}$$

$$\Delta\sigma_a = \Delta T C^e \Delta\boldsymbol{\varepsilon} - \Delta\lambda_a C^e \frac{\partial G}{\partial \boldsymbol{\sigma}_0} \tag{13}$$

$$\Delta K_a = \sqrt{\frac{2}{3}} \Delta\lambda_a H_p \left\| \frac{\partial G}{\partial \boldsymbol{\sigma}_0} \right\| \tag{14}$$

$$\sigma_a = \sigma_0 + \Delta\sigma_a \tag{15}$$

$$K_a = K_0 + \Delta K_a \tag{16}$$

$$\Delta\lambda_b = \frac{\left(\frac{\partial F}{\partial \boldsymbol{\sigma}_a}\right)^T C^e \Delta\boldsymbol{\varepsilon}}{\left(\frac{\partial F}{\partial \boldsymbol{\sigma}_a}\right)^T C^e \frac{\partial G}{\partial \boldsymbol{\sigma}_a} - \sqrt{\frac{2}{3}} \frac{\partial F}{\partial K_a} H_p \left\| \frac{\partial G}{\partial \boldsymbol{\sigma}_a} \right\|} \tag{17}$$

$$\Delta\sigma_b = \Delta T C^e \Delta\boldsymbol{\varepsilon} - \Delta\lambda_b C^e \frac{\partial G}{\partial \boldsymbol{\sigma}_a} \tag{18}$$

$$\Delta K_b = \sqrt{\frac{2}{3}} \Delta\lambda_b H_p \left\| \frac{\partial G}{\partial \sigma_a} \right\| \tag{19}$$

STEP 4: Calculate new values of stresses and hardening parameters and save them in the permanent memory by following the equations below:

$$\sigma_b = \sigma_0 + \frac{\Delta\sigma_a + \Delta\sigma_b}{2} \tag{20}$$

$$K_b = K_0 + \frac{\Delta K_a + \Delta K_b}{2} \tag{21}$$

STEP 5: Determining the relative error for the current sub-step using the following relationship:

$$R_n = \max\left\{\frac{\|\Delta\sigma_b - \Delta\sigma_a\|}{2\|\sigma_b\|}, \frac{|\Delta K_b - \Delta K_a|}{2|K_b|}, EEPS\right\} \quad (22)$$

In the above equation, EEPS is equal to the minimum acceptable error for the machine (for example 10^-14).

STEP 6: If $R_n > STOL$ (STOL is the acceptable error for Euler's second-order estimation tolerance and is usually a number between 10^{-3} and 10^{-6}). This means that the current sub-step fails and a smaller relative time factor should be selected using interpolation:

$$q = \max\left\{0.9\sqrt{\frac{STOL}{R_n}}, 0.1\right\} \quad (23)$$

$$\Delta T \leftarrow m\,ax\{q\Delta T, \Delta T_{\min}\}; \quad \Delta T_{\min} = 10^{-3}\ to\ 10^{-5} \quad (24)$$

Return to step 3.

STEP 7: If, $R_n < STOL$, the sub-step is ended successfully and the amount of stress and the hardening parameter are updated based on these equations:

$$\sigma = \sigma_b \quad (25)$$

$$K = K_b \quad (26)$$

STEP 8: If $|F(\sigma_b, k_b)| > FTOL$, 1), then the stress correction should be done using the error correction algorithm and finally the stress and hardening parameter should be placed on the yield surface (These steps are performed in a repeated cycle).

STEP 8.1: Selection of stress and hardening parameter values as input:

$$\sigma_{inp} = \sigma_b \quad (27)$$

$$K_{inp} = K_b \quad (28)$$

STEP 8.2: Calculation of the plastic coefficient:

$$\Delta\lambda = \frac{F(\sigma_{inp}, K_{inp})}{\left(\frac{\partial F}{\partial \boldsymbol{\sigma}_{inp}}\right)^T C^e \frac{\partial G}{\partial \boldsymbol{\sigma}_{inp}} - \sqrt{\frac{2}{3}}\frac{\partial F}{\partial K} H_p \left\|\frac{\partial G}{\partial \sigma_{inp}}\right\|} \quad (29)$$

STEP 8.3: Update of stress and hardening parameter values:

$$\Delta K = \sqrt{\frac{2}{3}}\Delta\lambda \left\|\frac{\partial G}{\partial \sigma_{inp}}\right\| \quad (30)$$

$$K = K_{inp} + \Delta K \quad (31)$$

$$\sigma = \sigma_{inp} - \Delta\lambda C^e \frac{\partial G}{\partial \sigma_{inp}} \quad (32)$$

STEP 8.4: If $|F(\sigma, K)| > |F(\sigma_{inp}, K_{inp})|$, then the correction of step 8.3 is canceled and the below correction is used:

$$\sigma = \sigma_{inp} - \frac{F(\sigma_{inp}, K_{inp})\left(\frac{\partial F}{\partial \sigma_{inp}}\right)}{\left(\frac{\partial F}{\partial \sigma_{inp}}\right)^T \frac{\partial F}{\partial \sigma_{inp}}} \quad (33)$$

$$K = K_{inp} \quad (34)$$

STEP 8.5: If $|F(\sigma, K)| < FTOL$ then go to the step 8.7, otherwise continue with the steps.

$$\sigma_{inp} = \sigma \quad (35)$$

$$K_{inp} = K \quad (36)$$

STEP 8.6: Return to step 8.1

STEP 8.7: Selection of final values of stress and hardening parameter:

$$\sigma_{new} = \sigma \quad (37)$$

$$K_{new} = K \quad (38)$$

STEP 9: Calculate the sub-step size for the next iteration using the relation:

$$q = \min\left\{0.9\sqrt{\frac{STOL}{R_n}}, 1.1\right\} \quad (39)$$

STEP 9.1: If the previous iteration has failed, the growth value of q is limited according to the following relationship

$$q = \min\{q, 1\} \quad (40)$$

STEP 9.2: The virtual time step size is updated and the new sub-step size is calculated and controlled according to the following relationships:

$$\Delta T \leftarrow q\Delta T \quad (41)$$

$$T \leftarrow T + \Delta T \quad (42)$$

$$\Delta T \leftarrow \max\{\Delta T, \Delta T_{\min}\} \quad (43)$$

$$\Delta T \leftarrow \min\{\Delta T, 1 - T\} \quad (44)$$

STEP 10: Output with updated stress and hardening parameter values at the end of virtual time step T=1.

In this way, by the introduced algorithm, the UMAT subprogram is coded in FORTRAN language and introduced to the ABAQUS software to be used during the analysis in the solution cycle.

3. Verification of WW-HFRC behavioral model

Any newly developed constitutive models of material should be investigated and verified based on test results under different stress paths, boundary conditions, and initial conditions through computer coding and modeling. In this study, uniaxial and true triaxial test results that were done by Chi et al. [25] were used for verification of the WW-HFRC constitutive model. So, the ABAQUS finite element software is used to simulate these tests, and the UMAT subprogram is coded in FORTRAN and introduced to the ABAQUS software.

3.1 Specifications of the samples

The mixing of the concrete samples tested under the 28-day strength of the fiber-free sample with a compressive strength of 60 Mpa is planned. In the samples with steel fibers, the same mixing design with a compressive strength of 60 MPa (C60), with fiber percentages of 0.5, 1, and 1.5% with an aspect ratio (length to diameter) of 30 was used. Finally, 75 samples were taken and tested after 28 days. The tests were carried out on the real three-axis device shown in Figure 4.

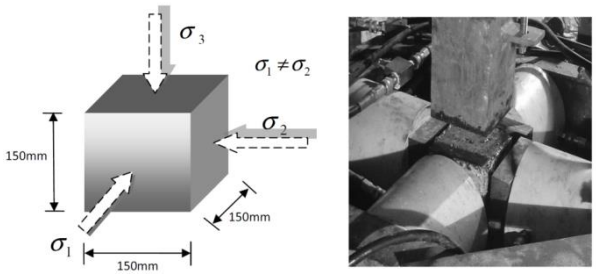

Fig. 4: The real triaxial test device of Chi et al.'s experiments [42]

3.2 Behavioral model parameters

Considering that the HFRC-WW behavior model has 12 independent parameters to define the behavior of concrete, the necessary parameters should be calibrated through tests. The coded model was based on the William-Warnke 5-parameter model. Seow et al. [29] have calibrated the parameters of the William-Warnke five-parameter model for fiber concrete in the order of Table 1 in a comprehensive study.

Table 1: The main parameters of the five-parameter William-Warnke model for fiber concrete.

$a_0 = b_0$	a_1	b_1	a_2	b_2
0.1732	− 1.455	− 0.788	− 0.1597	− 0.1746

To validate the coded model, real triaxial tests on a cubic sample with steel fiber percentages of 0.5, 1, and 1.5 have been used, which are related to Yin Chi's doctoral thesis, which is named in his thesis as the sample SA05, SA10 and SA15 are shown. According to his report, the modulus of elasticity and Poisson's ratio are 39000 MPa and 0.23 respectively. The effect of adding metal fibers in the HFRC-WW behavior model is determined by the parameter λ_{sf}, which is called the fiber reinforcement index (FRI). According to the relationships presented in the appendix, the parameters a, b, and ε_c are related to the hardening/softening of the model. The internal parameters of the HFRC-WW model are also presented in Table (2). Also, the initial value of the hardening parameter is K_0=0.4. The parameters related to the plastic potential function are presented based on the study of Yin Chi et al. [47].

Table 2: Internal parameters of HFRC-WW model for samples C60, SA05, SA10, SA15.

	C60	SA05	SA10	SA15
λ_{sf}	0	0.15	0.30	0.45
k_c	1	1.0084	1.0168	1.0252
k_t	1	1.012	1.024	1.036
a	1.099	1.121	1.145	1.142
b	0.12865	0.12675	0.12479	0.12429
ε_c	0.00204	0.00207	0.00210	0.00213
A	-11.25	-16.94	-16.1	-12.26
B	0.092	0.165	0.135	0.12

3.3 Simulation of the tests in the ABAQUS

The dimensions of the cubic samples are 15 cm according to the real samples (Figure 5-a) and the boundary conditions are applied to the sample according to the real triaxial device. The loading pattern in the real triaxial test as well as the simulation with ABAQUS is according to Figure 5-b. 8-node cubic elements with 8 Gauss points are used for modeling.

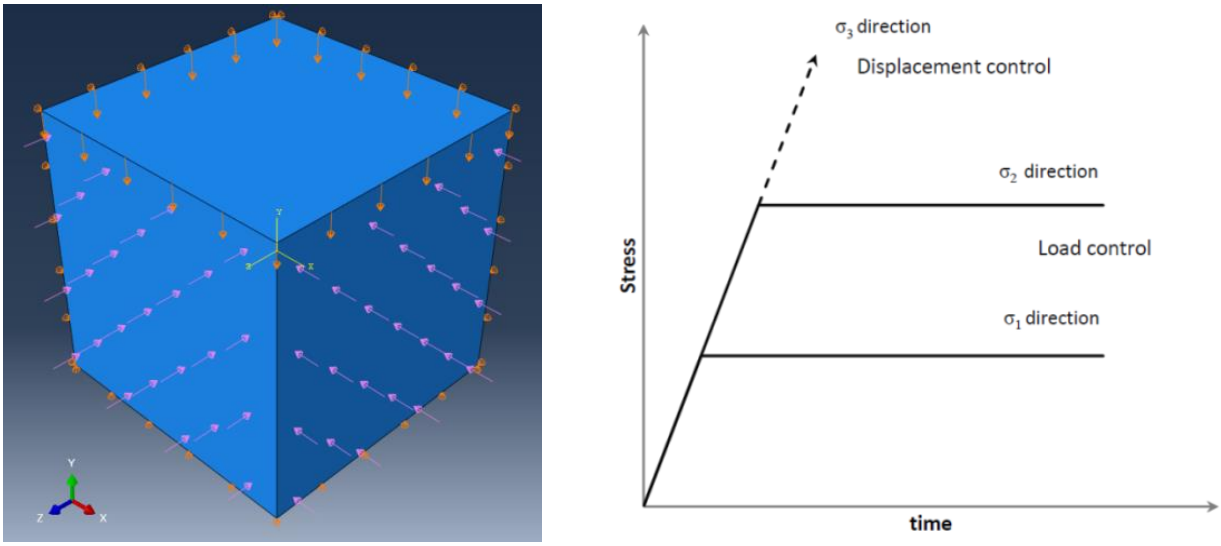

(a) (b)

Fig. 5: (a) Boundary conditions and loading of uniaxial cubic specimen in simulation with ABAQUS and (b) Loading pattern of cubic specimen in true triaxial test

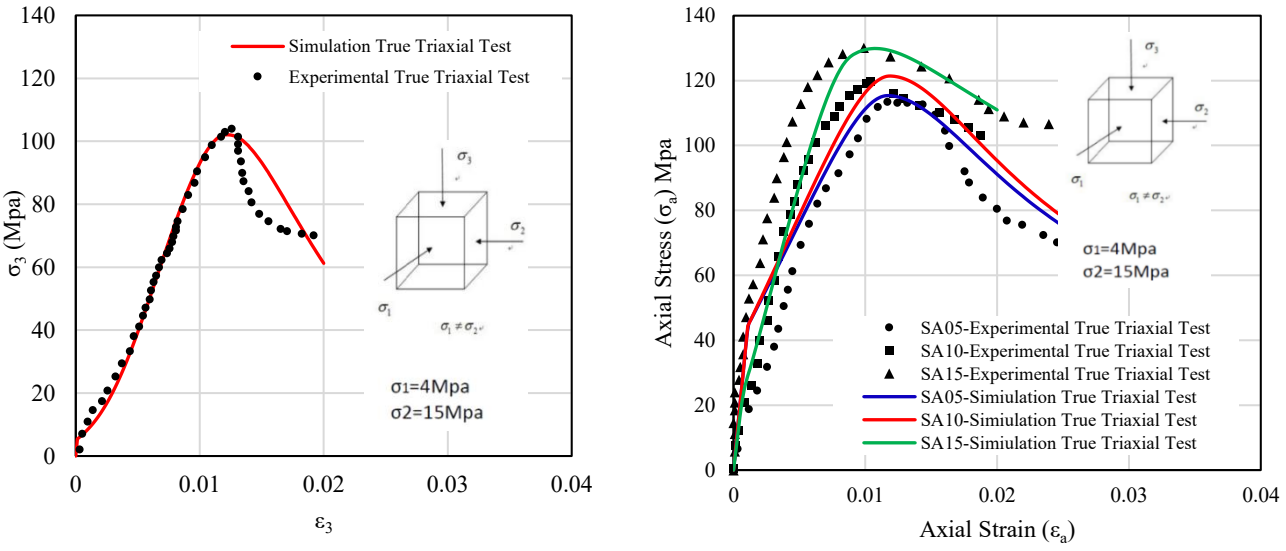

(a) (b)

Fig. 6: Comparison of stress-strain diagram of a real triaxial test and ABAQUS simulation with coded behavioral model. (a) For sample C60 and (b) for samples SA05, SA10, and SA15 with lateral stresses of 4 and 15 MPa.

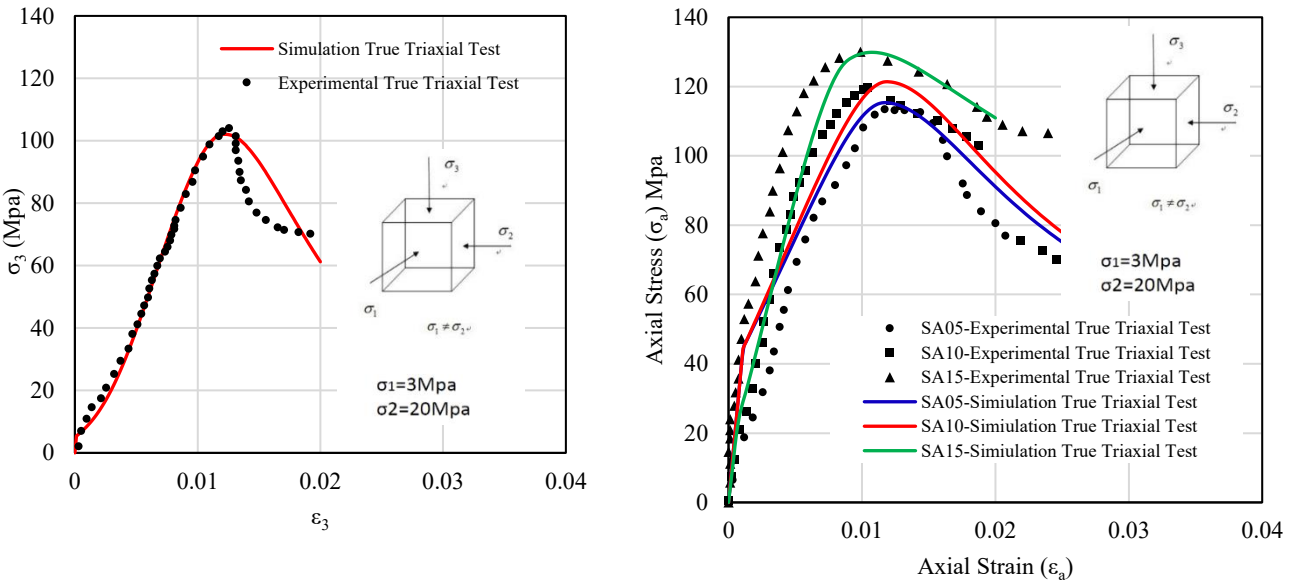

Fig. 7: Comparison of stress-strain diagram of a real triaxial test and ABAQUS simulation with coded behavioral model. (a) For sample C60 and (b) for samples SA05, SA10 and SA15 with lateral stresses of 3 and 20 MPa

The simulation of tests of samples SA05, SA10, and SA15 has been carried out for 2 sets of real triaxial tests with lateral stresses of 4 and 15 MPa as well as lateral stresses of 3 and 20 MPa. Figure 6 shows the modeling results of real tri-axial tests with lateral stresses of 4 and 15 MPa, and also presented in Figure 7 for lateral stresses of 3 and 20 MPa. It is noted that the behavioral model has a very high ability to simulate the behavior of fiber concrete and has shown soft and ductile failure well, and it can simulate the softening after failure.

4. Conclusion

In this research, the algorithm of integration and implementation of the generalized behavior model for fiber concrete was presented using the sub-step method. By using the presented algorithm, it was possible to create a tool for accurately simulating the behavior of fiber concrete following the experiments, and by adding the program to commercial software such as Abacus, it was possible to use it in projects related to the design of fiber concrete. Comparing the numerical simulation results using the nonlinear finite element method with the experimental results showed that the behavioral model can simulate the resistance behavior and deformation after fracture and softening until the residual strength is reached

References

[1] Mujalli, M. A., Dirar, S., Mushtaha, E., Hussien, A., & Maksoud, A. (2022). Evaluation of the Tensile Characteristics and Bond Behaviour of Steel Fibre-Reinforced Concrete: An Overview. Fibers, 10(12), 104.

[2] Nataraja, M. C., Dhang, N., & Gupta, A. P. (1999). Stress–strain curves for steel-fiber reinforced concrete under compression. Cement and concrete composites, 21(5-6), 383-390.

[3] Zhang, M. H., Li, L., & Paramasivam, P. (2004). Flexural toughness and impact resistance of steel-fibre-reinforced lightweight concrete. *Magazine of concrete research,* 56(5), 251-262.

[4] Song, P. S., & Hwang, S. (2004). Mechanical properties of high-strength steel fiber-reinforced concrete. *Construction and Building Materials*, 18(9), 669-673.

[5] Brandt, A. M. (2008). Fibre reinforced cement-based (FRC) composites after over 40 years of development in building and civil engineering. Composite structures, 86(1-3), 3-9.

[6] Shafei, B., Kazemian, M., Dopko, M., & Najimi, M. (2021). State-of-the-art review of capabilities and limitations of polymer and glass fibers used for fiber-reinforced concrete. *Materials*, 14(2), 409.

[7] Xu, L., Li, B., Chi, Y., Li, C., Huang, B., & Shi, Y. (2018). Stress-strain relation of steel-polypropylene-blended fiber-reinforced concrete under uniaxial cyclic compression. *Advances in Materials Science and Engineering*, 2018.

[8] Cucchiara, C., La Mendola, L., & Papia, M. (2004). Effectiveness of stirrups and steel fibres as shear reinforcement. *Cement and concrete composites*, 26(7), 777-786.

[9] Dancygier, A. N., & Savir, Z. (2006). Flexural behavior of HSFRC with low reinforcement ratios. *Engineering structures*, *28*(11), 1503-1512.

[10] Holschemacher, K., Mueller, T., & Ribakov, Y. (2010).

Effect of steel fibers on mechanical properties of high-strength concrete. *Materials & Design (1980-2015)*, *31*(5), 2604-2615.

[11] Olivito, R. S., & Zuccarello, F. A. (2010). An experimental study on the tensile strength of steel fiber reinforced concrete. *Composites Part B: Engineering*, *41*(3), 246-255.

[12] Ding, Y., You, Z., & Jalali, S. (2011). The composite effect of steel fibers and stirrups on the shear behavior of beams using self-consolidating concrete. *Engineering Structures*, *33*(1), 107-117.

[13] Negi, B. S., & Jain, K. (2022, May). Shear resistant mechanisms in steel fiber reinforced concrete beams: An analytical investigation. *In Structures* (Vol. 39, pp. 607-619). Elsevier.

[14] W.-F. Chen, D.-J. Han, Plasticity for structural engineers, *J. Ross Publishing*, 2007.

[15] Belarbi, A., & Hsu, T. T. (1995). Constitutive laws of softened concrete in biaxial tension compression. *Structural Journal*, 92(5), 562-573.

[16] Ansari, F., & Li, Q. (1998). High-strength concrete subjected to triaxial compression. *Materials Journal*, 95(6), 747-755.

[17] Attard, M. M., & Setunge, S. (1996). Stress-strain relationship of confined and unconfined concrete. *Materials Journal*, 93(5), 432-442.

[18] Hussein, A., & Marzouk, H. (2000). Behavior of high-strength concrete under biaxial stresses. *ACI Materials Journal,* 97(1), 27-36.

[19] Benipal, G. S., & Singh, A. K. (2006). Plasticity-based constitutive model for concrete in stress space. *Latin American Journal of Solids and Structures*, 417-441.

[20] Grassl, P., Lundgren, K., & Gylltoft, K. (2002). Concrete in compression: a plasticity theory with a novel hardening law. *International Journal of Solids and Structures*, 39(20), 5205-5223.

[21] Hammoud, R., Boukhili, R., & Yahia, A. (2013). Unified formulation for a triaxial elastoplastic constitutive law for concrete. *Materials*, 6(9), 4226-4248.

[22] Hsu, L. S., & Hsu, C. T. (1994). Stress-strain behavior of steel-fiber high-strength concrete under compression. *Structural Journal*, 91(4), 448-457.

[23] Murugappan, K., Paramasivam, P., & Tan, K. H. (1993). Failure envelope for steel-fiber concrete under biaxial compression. *Journal of materials in civil engineering,* 5(4), 436-446.

[24] Hu, X. D., Day, R., & Dux, P. (2003). Biaxial failure model for fiber reinforced concrete. *Journal of materials in civil engineering*, 15(6), 609-615.

[25] Chi, Y., Xu, L., & Yu, H. S. (2014). Plasticity model for hybrid fiber-reinforced concrete under true triaxial compression. *Journal of Engineering Mechanics*, 140(2), 393-405.

[26] Tran, T. T., Pham, T. M., Tran, D. T., Ha, N. S., & Hao, H. (2024). Modified plastic damage model for steel fiber reinforced concrete. *Structural Concrete*.

[27] Wang, H., Li, L., & Du, X. (2024). A thermo-mechanical coupling model for concrete including damage evolution. International Journal of Mechanical Sciences, 263, 108761.

[28] Golpasand, G. B., & Farzam, M. (2023). Triaxial behavior of concrete containing recycled fibers-an experimental study. Construction and Building Materials, 406, 133430.

[29] Seow, P. E. C., & Swaddiwudhipong, S. (2005). Failure surface for concrete under multiaxial load—A unified approach. *Journal of materials in civil engineering*, 17(2), 219-228.

[30] Yun, H. D., Yang, I. S., Kim, S. W., Jeon, E., Choi, C. S., & Fukuyama, H. (2007). Mechanical properties of high-performance hybrid-fibre-reinforced cementitious composites (HPHFRCCs). *Magazine of Concrete Research,* 59(4), 257-271.

[31] Di Prisco, M., Plizzari, G., & Vandewalle, L. (2009). Fibre reinforced concrete: new design perspectives. *Materials and structures*, 42, 1261-1281.

[32] K.J. Willam, E.P. Warnke, Constitutive model for the triaxial behaviour of concrete, in: Proc., Seminar on Concrete Structures Subjected to Triaxial Stresses, *Int. Association of Bridge and Structural Engineering, Zurich, Switzerland, 1974.*

[33] Slater, E., Moni, M., & Alam, M. S. (2012). Predicting the shear strength of steel fiber reinforced concrete beams. *Construction and Building Materials*, *26*(1), 423-436.

[34] Sabetifar, H., & Nematzadeh, M. (2021, December). An evolutionary approach for formulation of ultimate shear strength of steel fiber-reinforced concrete beams using gene expression programming. *In Structures* (Vol. 34, pp. 4965-4976). Elsevier.

[35] Lu, X., & Hsu, C. T. T. (2006). Behavior of high strength concrete with and without steel fiber reinforcement in triaxial compression. *Cement and Concrete Research*, *36*(9), 1679-1685.

[36] Pantazopoulou, S. J., & Zanganeh, M. (2001). Triaxial tests of fiber-reinforced concrete. *Journal of Materials in Civil Engineering*, *13*(5), 340-348.

[37] Farnam, Y., Moosavi, M., Shekarchi, M., Babanajad, S. K., & Bagherzadeh, A. (2010). Behaviour of slurry infiltrated fiber concrete (SIFCON) under triaxial compression. *Cement and concrete research*, *40*(11), 1571-1581.

[38] Jiang, J. F., Xiao, P. C., & Li, B. B. (2017). True-triaxial compressive behaviour of concrete under passive confinement. *Construction and Building Materials*, *156*, 584-598.

[39] Abbas, Y. M., & Khan, M. I. (2023). Prediction of compressive stress–strain behavior of hybrid steel–polyvinyl-alcohol fiber reinforced concrete response by fuzzy-logic approach. Construction and Building Materials, 379, 131212.

[40] Raza, A., Selmi, A., Arshad, M., Elhadi, K. M., & Alashker, Y. (2024). Tests and modeling of hybrid fiber-reinforced geopolymer concrete elements having BFRP helix: An application for sustainable built environment. Journal of Building Engineering, 82, 108229.

[41] Willam, K. J. (1974). Constitutive model for the triaxial behavior of concrete. *In IABSE Seminar on Concrete Structure*

subjected Triaxial Stresses (pp. 1-30).

[42] Chi, Y. (2012). Plasticity theory based constitutive modelling of hybrid fiber reinforced concrete *(Doctoral dissertation, University of Nottingham).*

[43] Blanco, A., Pujadas, P., Cavalaro, S., De la Fuente, A., & Aguado, A. (2014). Constitutive model for fiber reinforced concrete based on the Barcelona test. *Cement and Concrete Composites*, *53*, 327-340.

[44] Mihai, I. C., Jefferson, A. D., & Lyons, P. (2016). A plastic-damage constitutive model for the finite element analysis of fiber reinforced concrete. *Engineering Fracture Mechanics*, *159*, 35-62.

[45] Chi, Y., Yu, M., Huang, L., & Xu, L. (2017). Finite element modeling of steel-polypropylene hybrid fiber reinforced concrete using modified concrete damaged plasticity. *Engineering Structures*, *148*, 23-35.

[46] Liang, X., & Wu, C. (2018). Meso-scale modelling of steel fiber reinforced concrete with high strength. *Construction and Building Materials*, *165*, 187-198.

[47] Ribeiro, M. L., Vandepitte, D., & Tita, V. (2013). Damage model and progressive failure analyses for filament wound composite laminates. Applied Composite Materials, 20, 975-992.

[48] Chi, Y., Xu, L., & Yu, H. S. (2014). Constitutive modeling of steel-polypropylene hybrid fiber reinforced concrete using a non-associated plasticity and its numerical implementation. *Composite Structures*, 111, 497-509.

[49] Sloan, S. W., Abbo, A. J., & Sheng, D. (2001). Refined explicit integration of elastoplastic models with automatic error control. *Engineering Computations*, 18(1/2), 121-194.

[50] Dowell, M., & Jarratt, P. (1972). The "Pegasus" method for computing the root of an equation. *BIT Numerical Mathematics*, 12, 503-508.